frontiers | Frontiers in Environmental Science

TYPE Original Research
PUBLISHED 02 March 2023
DOI 10.3389/fenvs.2023.1112019

Check for updates

OPEN ACCESS

EDITED BY
Ahmed El Nemr,
National Institute of Oceanography and Fisheries (NIOF), Egypt

REVIEWED BY
Rachid Hsissou,
Chouaïb Doukkali University, Morocco
Kovo Godfrey Akpomie,
University of Nigeria, Nigeria

*CORRESPONDENCE
S. Jodeh,
sjodeh@najah.edu
S. Saoiabi,
s.saoiabi@yahoo.com
K. Azzaoui,
k.azzaoui@yahoo.com

SPECIALTY SECTION
This article was submitted to Water and Wastewater Management, a section of the journal Frontiers in Environmental Science

RECEIVED 30 November 2022
ACCEPTED 13 February 2023
PUBLISHED 02 March 2023

CITATION
El Hammari L, Hamed R, Azzaoui K, Jodeh S, Latifi S, Saoiabi S, Boukra O, Krime A, Boukra A, Saoiabi A, Hammouti B, Khan MM, Sabbahi R, Hanbali G, Berisha A, Taleb M and Dagdag O (2023), Optimization of the adsorption of lead (II) by hydroxyapatite using a factorial design: Density functional theory and molecular dynamics.
Front. Environ. Sci. 11:1112019.
doi: 10.3389/fenvs.2023.1112019

COPYRIGHT
© 2023 El Hammari, Hamed, Azzaoui, Jodeh, Latifi, Saoiabi, Boukra, Krime, Boukra, Saoiabi, Hammouti, Khan, Sabbahi, Hanbali, Berisha, Taleb and Dagdag. This is an open-access article distributed under the terms of the Creative Commons Attribution License (CC BY). The use, distribution or reproduction in other forums is permitted, provided the original author(s) and the copyright owner(s) are credited and that the original publication in this journal is cited, in accordance with accepted academic practice. No use, distribution or reproduction is permitted which does not comply with these terms.

Optimization of the adsorption of lead (II) by hydroxyapatite using a factorial design: Density functional theory and molecular dynamics

L. El Hammari[1], R. Hamed[2], K. Azzaoui[3]*, S. Jodeh[2]*, S. Latifi[1,4], S. Saoiabi[1]*, O. Boukra[1], A. Krime[1], A. Boukra[1], A. Saoiabi[1], B. Hammouti[5], M. M. Khan[6], R. Sabbahi[7], G. Hanbali[2], A. Berisha[8], M. Taleb[3] and O. Dagdag[9]

[1]Laboratory of Applied Chemistry of Materials, Department of Chemistry, Faculty of Sciences, Mohammed V University in Rabat, Rabat, Morocco, [2]Department of Chemistry, An-Najah National University, Nablus, Palestine, [3]Laboratory of Engineering, Electrochemistry, Modeling and Environment, Faculty of Sciences, Sidi Mohamed Ben Abdellah University, Fez, Morocco, [4]Laboratory REMTEX, ESITH (Higher school of textile and clothing industries), Casablanca, Morocco, [5]Laboratory of Industrial Engineering, Energy and Environment (L13E) SUPMTI, Rabat, Morocco, [6]Chemical Sciences, Faculty of Science, Universiti Brunei Darussalam, Gadong, Brunei Darussalam, [7]Laboratory of Development and Valorization of Resources in Desert Zones, Higher School of Technology, University of Ibn Zohr, Laayoune, Morocco, [8]Department of Chemistry, Faculty of Natural and Mathematics Science, University of Prishtina, Prishtina, Kosovo, [9]Centre for Materials Science, College of Science, Engineering and Technology, University of South Africa, Johannesburg, South Africa

Hydroxyapatite (HAp) synthesized through a wet chemical procedure was used to adsorb lead (II) from an aqueous solution. HAp was characterized using Fourier transform infrared, X-ray diffraction, Brunauer–Emmett–Teller analysis, and scanning electron microscopy. The removal of Pb^{+2} was investigated using the factorial design approach to investigate the efficiency of different Pb^{+2} concentrations, adsorption contact time, and HAp mass. The greatest Pb^{+2} removal (98.94%) was obtained at a starting concentration of 50 mg/L, a contact period of 15 min, and a pH of 8. At 323 K, the isothermal adoption module was fitted to the Langmuir isotherms with a regression coefficient (R^2) of 0.96. The thermodynamic calculations revealed that the adsorption process was exothermic, spontaneous, and predominantly dominated by chemisorption. Furthermore, the maximum adsorption capacity (Q_{max}) at equilibrium was 90.18 mg/g, and the adsorption kinetics was specified by a pseudo-second-order kinetic model. Density functional theory and theoretical studies showed that the results of the experiment were correlated by the observation of a much higher negative E_{ads} value for the lead ion adsorbate molecules as they attached to the surface of the adsorbent.

KEYWORDS

adsorption, factorial design, hydroxyapatite, lead (II), optimization, pollution

1 Introduction

Industrial discharge containing heavy metals is a threat to the environment and the well-being of life, and can cause serious problems (Ajibade et al., 2021). Water is polluted by mining, agricultural, and domestic activities (Ukaogo et al., 2020; Singh et al., 2021).

Heavy metals are naturally occurring non-biodegradable components of the Earth's crust that can be found in surface waters in dissolved, colloidal, or particle forms (Saravanan et al., 2021). Heavy metals can accumulate in living organisms (Mehana et al., 2020) and, in larger quantities, can induce poisoning and endanger human, animal, and environmental health (Saoiabi et al., 2013). Among toxic heavy metals, lead is one of the most commonly occurring in the environment, particularly in water resources (Vardhan et al., 2019). This cumulative toxin mostly accumulates in the bones, which can lead to consequences including excessive blood pressure and brain damage in humans (Olatunji-Ojo et al., 2020).

The pollution of water resources by lead ions (Pb^{2+}) is a major issue, and countries worldwide are at risk due to a lack of wastewater treatment solutions. However, researchers have developed methods for eliminating Pb^{2+} from water, such as chemical precipitation (Chen et al., 2018; Mohammed and Selman 2018; Yang Z et al., 2019; Wu et al., 2021), ion exchange (Wu et al., 2021), solvent extraction (El Hammari et al., 2006a), adsorption (Nyairo et al., 2018), and reverse osmosis (Saravanan et al., 2021) methods. The most universal of available physical methods is the adsorption technique, as it can be used for a wide variety of different treatments and is fast, efficient, and inexpensive to set up and operate (Rafatullah et al., 2010; Said et al., 2020).

A sewage treatment facility can generate large volumes of sludge containing enormous amounts of humic acid (HA). The present study isolated HA and investigated its ability to adsorb Pb^{2+} from a solution (Dai et al., 2021). Pb^{2+} was concentrated in water using alkaline layered titanate ($Cs_2Ti_5O_{11}$) (Sruamsiri and Ogawa 2022). Previous researchers developed a graphene composite hydrogel containing tiny pores with large surface area from natural cryptocrystalline graphite, which was used to adsorb Pb^{2+} from an aqueous solution (El Hammari et al., 2007; Sruamsiri and Ogawa 2022).

Hydroxyapatite (HAp) is an important component of methods for hazardous pollutants adsorption in the field of water and wastewater treatment. HAp is easily produced on a large scale, allowing for the scaling up of technologies while also being swiftly regenerated. Thus, metals may be recovered without costly techniques. HAp is also readily adjustable for specific applications; this remarkable adaptability allows its use in the most difficult operating conditions. HAp adsorbents are effective in absorbing common pollutants such as Pb^{2+}, Cu^{2+}, Cd^{2+}, Ni^{2+}, etc.

Previous studies applied "one variable at a time" tests to investigate the individual influence of numerous parameters on the adsorption process. However, factorial experimental design can yield substantial information while reducing the number of trials, time, and overall research expenses. The most significant advantages of this approach are that it can determine the influence of individual parameters, their relative importance, and the interaction of two or more factors. However, research is limited regarding the use of HAp for Pb^{2+} adsorption.

Theoretical research such as density functional theory (DFT) and Monte Carlo (MC) dynamics have provided a thorough understanding of lead ion adsorption and how it is related to the HAp surface (Hsissou 2021; Hsissou et al., 2021; El Amri et al., 2023).

The present study optimized the process parameters for lead removal using HAp. First, we used a wet chemical procedure to prepare HAp as an absorbent. A full factorial design was applied to determine the influence of various parameters (initial Pb^{2+} concentration, contact time, and adsorbent mass) and their interactions on the removal efficiency of lead. We then assessed the importance of HAp as an adsorbent for Pb^{2+} removal from water. We also applied molecular dynamic MC simulations and DFT to explore the absorption mechanism and investigate the interaction between Pb^{+2} and the modeled HAp surface.

2 Materials and methods

2.1 Materials

HAp was produced as previously described. Analytical-grade calcium hydroxide ($Ca(OH)_2$), ammonium dihydrogen phosphate ($NH_4H_2PO_4$), and lead nitrate ($Pb(NO_3)_2$) were obtained from Sigma-Aldrich at purities exceeding 99%.

2.2 HAp synthesis

Porous HAp was synthesized using a wet chemical technique, as previously described (El Hammari et al., 2007). Two solutions were prepared separately. Solution A was made up of 14.82 g $Ca(OH)_2$ in 200 ml of distilled water, while Solution B was made up of 13.80 g $NH_4H_2PO_4$ in 100 ml of distilled water. Both solutions were agitated for 90 min at room temperature until all compounds were dissolved. The two solutions were then combined for 48 h, followed by vacuum filtration and drying overnight at 100°C.

2.3 HAp characterization

The Fourier transform infrared (FT-IR) spectra of various materials in the 400–4,000 cm^{-1} range were obtained using a spectrophotometer (Bruker counter, IFS 66v FT-IR), while their surface morphologies were determined using a scanning electron microscope (3.0 KV SE(U), SU 8020). To study the crystalline structure of HAp, the surface area was measured and characterized using the Brunauer–Emmett–Teller (BET) method to characterize the surface area during the adsorption process for adsorption data in the range of 0.05–0.25 and Barret-Joyner-Halenda approximation (BJH) to determine the distribution in mesoporous range. Finally, X-ray diffraction (XRD model Philips PW131 using Cu Kα radiation) was used to study the phase and structure.

TABLE 1 Low and high levels of experimental factors in the 2^3 full factorial design.

Factor	Symbol	Levels	
		-1	+1
Initial concentration of Pb^{2+} (mmol/L)	A	0.2	8
Contact Time (min)	B	5	240
Mass of HAp (g)	C	0.1	0.4

2.3.1 Porosity measurement

The Brunauer–Emmett–Teller (BET) (Asap 2020 Porosimeter, Micromeritics, Manchester, United Kingdom) technique was used to measure the HAp surface area and pore size distribution.

2.4 Factors affecting Pb^{2+} adsorption on the HAp adsorbent

Adsorption depends on various parameters. Pb^{2+} adsorption was measured by individually varying each of the following parameters.

2.4.1 pH

To assess the effects of pH on adsorption, 0.2 g samples of HAp were weighed and immersed in 100 ml Pb^{2+} solutions at 50 mg/L and pH values ranging from 2 to 11. The mixture was then shaken at 150 rpm for 60 min before the samples were centrifuged and further examined.

2.4.2 Time effects on adsorption

To assess the effects of time on adsorption, 0.2 g samples of HAp were weighed and immersed in 50 ml Pb^{2+} solutions at 50 mg/L and a pH of 8 and shaken at 150 rpm for time durations ranging from 1 to 8 h. The mixtures were then centrifuged before further analysis.

2.4.3 Lead concentration effects on adsorption

To assess the effects of lead concentration on adsorption, 0.2 g samples of HAp were weighed and immersed in 50 ml Pb^{2+} solutions of varying concentrations at a pH level of 8 and shaken at 150 rpm for 60 min. The mixtures were then centrifuged before further analysis.

2.4.4 Temperature effects on adsorption

To assess the effects of temperature on adsorption, 0.2 g samples of HAp were weighed and immersed in 50 ml of a 50 mg/L Pb^{2+} solutions at a pH of 8 and shaken at 150 rpm for 60 min. The mixtures were then centrifuged before further analysis.

2.5 Adsorption

To measure the concentration of Pb^{2+} solution adsorbed, the prepared sample solutions were quantified and compared to a standard solution of lead nitrate. The absorbance was determined using flame atomic absorption spectroscopy (FAAS). To investigate

TABLE 2 Plan matrix used in the present study.

Run	Factor 1: A (mmol/L)	Factor 2: B	Factor 3: C	Response: R
		(min)	(g)	(%)
1	0.2	240	0.146	90
2	0.2	240	0.4	100
3	7.142	240	0.352	47.5
4	7.142	240	0.1	31.7
5	4.217	5	0.208	65
6	4.217	5	0.4	70
7	8	121.325	0.205	40.3
8	8	121.325	0.4	42.5
9	3.71	133.075	0.2635	67.5
10	3.71	133.075	0.1	65.7
11	3.632	134.25	0.257	67.5
12	3.632	134.25	0.257	67.5
13	0.2	28.5	0.1	40
14	0.2	28.5	0.355	80
15	8	5	0.3055	82
16	8	5	0.1	33

-Fit statistics

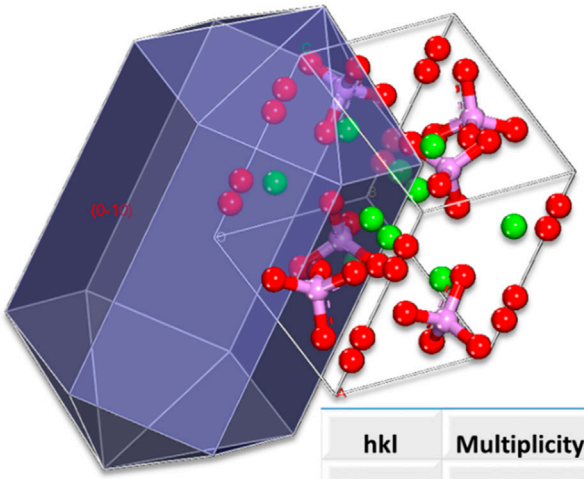

hkl	Multiplicity	dhkl	Distance	% Total facet area
{ 1 -1 0}	6	8.158	12.251	64.452
{ 1 -1 1}	12	5.259	19.012	35.547

FIGURE 1
BFDH for the HAp unit cell and the derived results.

the nature of the adsorption process, the thermodynamics of the adsorption process were explored (El-Bahy and El-Bahy 2016; Huang and Pan 2016; Nazari et al., 2016).

The Pb^{2+}adsorption behaviors on the prepared HAp were assessed using Eqs 1, 2 to calculate the removal efficiency, which is presented as R%, and the adsorption capacity, which is presented as Q_e:

$$R(\%) = \frac{C_{0-C_e}}{C_0} 100 \quad (1)$$

$$Q_e = \frac{C_0 - C_e}{W} V \quad (2)$$

where C_0 and C_e are the initial and equilibrium Pb^{2+} concentration (mg/L), respectively, Qe (mg/L) is the equilibrium adsorption capacity, W is the adsorbent weight (mg), and V is the solution volume (ml).

2.5.1 Adsorption isotherm

Adsorption isotherms are useful for analyzing the interactions and collisions between adsorbate and adsorbent throughout the uptake process (El Hammari et al., 2006b). Langmuir and Freundlich isotherm models are the most extensively used. Eqs 3, 4 can be used to calculate the non-linear forms of the Langmuir and Freundlich models (Hanbali et al., 2020a; Kadiri et al., 2021; Hamed et al., 2022).

$$\text{Langmuir isotherm model: } \frac{C_e}{Q_e} = \frac{1}{q_{max}} C_e + \frac{1}{q_{max} K_L} \quad (3)$$

$$\text{Freundlich isotherm model: } \ln(Q_e) = \ln K_F + \frac{1}{n} \ln C_e \quad (4)$$

The constants Q_e (mg g^{-1}) and q (mg g^{-1}) represent the equilibrium and the saturated adsorption capacity, respectively; K_L (mg $^{-1}$) is the Langmuir constant associated with the adsorbent's affinity; K_F (mg L^{-1}) and n represent the Freundlich constants; and C_e (mg L^{-1}) represents the equilibrium concentration of targeted metal ions.

The dimensionless constant for the separation factor shown in Eq. 5 is used to determine if the adsorption is favorable or unfavorable when applying the Langmuir isotherm model

$$R_L = \frac{1}{1 + K_{L C_0}} \quad (5)$$

where K_L represents the Langmuir constant and the constant C_o is the initial adsorbate concentration. In general, when the R_L value is >1, the adsorption is unfavorable. Adsorption is also favorable for values between 1 and 0. An R_L value of 1 indicates linear adsorption. Non-ideal adsorption, including heterogeneous surface energy systems, is represented by the Freundlich isotherm in Eq. 6:

$$Q_e = K_F C_e^{1/n} \quad (6)$$

where K_F (L mg^{-1}) represents the Freundlich constant and 1/n is the adsorption intensity. In general, when the 1/n value is between 0.1 and 0.5, the adsorption is favorable, while a $1/n$ value >2 indicates unfavorable adsorption (Hanbali et al., 2020b; Algarra et al., 2022).

2.5.2 Adsorption kinetics

To explore the adsorption rates and define the adsorption mechanism of Pb^{2+} on the HAp surface, both pseudo-first-order and pseudo-second-order kinetic models with intraparticle diffusion were studied. The linearized forms of the rate equations (Algarra et al., 2022), were estimated according to Eqs 7–10.

$$\ln(Q_e - Q_t) = \ln Q_e - K_1 t \quad (7)$$

$$\frac{t}{Q_t} = \frac{1}{K_{2Q_e^2}} + \frac{t}{Q_e} \quad (8)$$

$$Q_t = K_{id} t^{1/2} + Z \quad (9)$$

TABLE 3 Three-variable factorial design matrix with actual and expected responses for Pb^{2+} removal by Hap.

Run order	Actual value	Predicted value	Residual
1	90.00	91.53	-1.53
2	100.00	99.04	0.961
3	47.50	46.64	0.855
4	31.70	32.02	-0.318
5	65.00	63.47	1.53
6	70.00	73.33	-3.33
7	40.30	41.73	-1.43
8	42.50	42.84	-0.339
9	67.50	68.85	-1.35
10	50.00	44.28	5.72
11	67.50	68.89	-1.39
12	67.50	68.89	-1.39
13	40.00	41.54	-1.54
14	80.00	77.92	2.08
15	70.00	66.20	3.80
16	33.00	35.33	-2.33

$$\ln\frac{K(T_2)}{K(T_1)} = \frac{Ea}{R}\left(\frac{1}{T_1} - \frac{1}{T_2}\right) \quad (10)$$

$$\mathrm{Ln}\,(1-F) = -K_{\mathrm{fd}}{}^{\star}\mathrm{t} \quad (11)$$

where both Q_e and Q_t represent the adsorption capacities (mg/g) at equilibrium with variable times (t, min). K_1 is usually used as the pseudo-first-order rate constant (min^{-1}), while K_2 is for the pseudo-second-order rate constant (g/mg.min). K_{id} represents the intra-particle diffusion rate constant (mg $g^{-1}min^{-1/2}$) and Z (mg/g) is used to calculate the thickness of the boundary layer. In Eq. 10, *Ea* represents the activation energy.

In Eq. 11, F represents the fractional achievement of equilibrium ($F = Q_t/Q_e$) and K_{fd} (min^{-1}) represents the rate of film diffusion.

The effects of different temperatures on the sorption process were investigated using the thermodynamic test. Eqs 12–14 were used to calculate the thermodynamics parameters, including the Gibbs free energy change (ΔG^0 in kJ mol^{-1}), the standard enthalpy of adsorption (ΔH^0 in kJ mol^{-1}), and the standard entropy change (ΔS^0 in J mol^{-1} K^{-1}):

$$K_c = C_{ads}/C_e \quad (12)$$

$$\Delta G^0 = -RT\ln K_c \quad (13)$$

$$\ln K_d = \frac{\Delta S}{R} - \frac{\Delta H}{RT} \quad (14)$$

where K_c is a thermodynamic constant, C_{ads} is the equilibrium Pb^{2+} adsorbed quantity (mg/L), C_e is the equilibrium concentration (mg/L), T is the solution temperature (K), and R is the ideal gas constant (J/mol_K). The slope and intercept of the plot of ln (K_d) vs 1/T are used to determine the numerical values of ΔH^0 and ΔS^0 (Kwak et al., 2019).

2.5.3 Design and optimization

Researchers have designed software to study the influence of experimental parameters (initial concentrations of Pb^{2+}, contact time, and mass of HAp) on Pb^{2+} adsorption. Statistical optimization with full factorial experimental design is commonly used to determine the boundary conditions that maximize the output of the desired products. Using a proper design matrix, we can obtain a regression equation that highlights the effect of individual parameters and their relative importance in a given operation/process. The interactional effects of two or more variables can also be determined. In our study, all experiment runs were carried out according to the design matrix, which depended on the number of variables to be investigated. Each variable had three levels, denoted by -1 for the lowest, and +1 for the highest (Table 1). The matrix used in this investigation included 16 passages. All the trials were performed at room temperature. Table 2 shows the times at which the experimental samples were taken from the shaker.

Several parameters and constants were used to study the statistics (Supplementary Table S13):

- Standard deviation (Std Dev) and the square root of the residual mean square (Root MSE).
- Overall average of all the response data (mean).
- Coefficient of variation (CV) used to determine the percentage of the mean.
- R-squared, which is used to represent the variation around the mean that is explained by a model
- Adj R-squared, which is used to explain the variation and changes around the mean of the model, and is adjusted for the number of terms in the model.

2.6 DFT calculation

The Dmol3 module of the Materials Studio (MatS) software was used to acquire the results of quantum chemical modeling using the M-06 L (Zhao and Truhlar 2008; Akartasse et al., 2017) exchange-correlation function and the double numeric quality with polarization (DNP) basis (Ben Hadj Ayed et al., 2019; Molhi et al., 2021) set with the COSMO model for aqueous phase (Barone and Cossi 1998; Klamt 2018; Berisha 2019). The calculations were performed on the monohydroxylated surface of a HAp unit cell. The results of the vibrational analysis demonstrated that the place on the potential energy surface with the lowest amount of energy was the minimal point (Berisha et al., 2017; Berisha 2021). The interaction energies were estimated from equations described previously (Hsissou et al., 2020a; Berisha 2021; Berisha and Seydou 2022).

2.7 Monte Carlo and molecular dynamics

Monte Carlo (MC) simulations were used to investigate the interactions between Pb^{2+} and the modeled HAp surface in the simulated adsorption environment. The size of the model used in the calculations was: 37.684 Å × 27.520 Å x 11.494 Å thick (Figure 1, Part A). The MC calculations were performed in the simulation box filled with a Pb(II) ion and 1,250 water molecules. The commonly

TABLE 4 Results of variance analysis (ANOVA).

Source	Term df	Error df	F-value	*p*-value	Significant
Whole-plot	5	6.00	59.05	<0.0001	
a-A	1	6.00	193.96	<0.0001	
b-B	1	6.00	5.15	0.0638	
Ab	1	6.00	72.61	0.0001	
a^2	1	6.00	1.31	0.2962	
b^2	1	6.00	7.29	0.0356	
Subplot	4	6.00	33.49	0.0003	Significant
C-C	1	6.00	80.51	0.0001	
a-C	1	6.00	1.61	0.2515	
b-C	1	6.00	10.88	0.0164	
C^2	1	6.00	25.71	0.0023	

employed universal force field was used for the simulation calculations (Hsissou et al., 2020b; Berisha and Seydou 2022). HAp with a (1–1 0) orientation was based on Bravais–Friedel–Donnay Harker (BFDH) crystal morphology calculation (Figure 1) as the most stable HAp structure (Rahimi et al., 2022). The MD simulations were performed at 295 K, with an NVT ensemble, a time step of 1 fs, and a simulation time of 800 ps (Hsissou et al., 2020a; Abdelwedoud et al., 2022; Hu et al., 2022).

2.8 Adsorbent regeneration

After reaching the saturation state for the adsorbent presented by the equilibrium, the reverse process is desorption, in which the adsorbate is removed from the adsorbent site; despite the lower efficiency of removal, the substrate can be used for additional adsorption cycles.

A mixture of 10 mg adsorbent (HAp) and 10 ml of 50 ppm Pb^{+2} at a pH of 8 was shaken in a water bath for 15 min at 25°C. The FAAS measurements for the filtrate were then determined.

After each adsorption process, the adsorbent was washed with 0.1 M HCl solution and then with distilled water before being left to dry for 24 h before repeating the adsorption process. The same recovery technique was used for each regenerated adsorbent to prove that HAp could be used several times with limited effect on the percentage removal of Pb^{+2}.

3 Results and discussion

3.1 Infrared analysis

The infrared spectrum of the HAp structure was investigated (Supplementary Figure S1), which showed the absorption bands attributed to the apatite lattice's PO_4^{3-} and OH^- groups. PO_4^{3-} ion absorption bands are distinguished by two absorption ranges: 1,100–900 cm^{-1} and 600–500 cm^{-1}. The first domain bands correspond to the symmetric and antisymmetric vibrations of the P-O bond, whereas the second domain bands correspond to the deformation vibrations of the O-P-O bond. Low-intensity bands are also observed at 1,560 and 1,430 cm^{-1}, which correspond to the vibrational frequencies of CO_3^{2-} carbonate ions and HPO_4^{2-} groups. Furthermore, the distinctive absorption bands at the vibration frequencies of the OH^- ions in the apatitic lattice occur at 3,560 cm^{-1} (Azzaoui et al., 2013).

3.2 Specific surface

Both the mesoporous and microporous morphologies of HAp were analyzed.

Based on the principle of the adsorption-desorption of nitrogen gas by BET analysis, nitrogen gas can be adsorbed on the surface; thus, it can be used for the analysis of both surface area and porosity of synthesized HAp. Nitrogen gas adsorption was used to measure the depth profile of the pores in addition to the desorption isotherm method. The adsorption and desorption curves showed that they were not reversible and hysteresis was observed between the curves. The adsorption-desorption showed a

type IV curve with a hysteresis loop without any indication of a mesoporous material (Supplementary Figure S2), while the isotherm curve did not show a closed hysteresis loop. The BET surface area of the synthesized HAp sample showed a minimum area of 8.124 ± 0.0214 m^2/g due to its non-porous nature, with an average pore size porosity of 2.15 nm (Azzaoui et al., 2013).

3.3 X-ray diffraction

The X-ray diffraction pattern of HAp is shown in Supplementary Figure S3. The XRD analysis showed that prepared the products were well-crystallized and consisted of a single phase with an apatite structure. The lines of the XRD diagram were all indexed in the hexagonal system of the space group $P6_{3/m}$, with crystalline parameters of a = 9.432 and c = 6.883 Å (Khalaf et al., 2021). The results and diffraction were consistent with those of the ASTM data (JCPDS) file (no. 09–0,432) for HAp.

No calcium hydroxide or calcium phosphate peaks were observed, which are considered pollutants. Thus, we concluded that we generated phase-pure HAp under the experimental conditions. All acquired peaks were in plane (0 0 2) (2 1 1) (1 1 2), and (3 0 0), with very thin and sharp peaks indicating good HAp synthesis and crystallization. The (002) reflection peak from the various XRD patterns was used to calculate the HAp crystallite size using the Debye–Scherrer equation.

3.4 Scanning electron microscopy (SEM)

SEM was used to study the microstructure of the HAp composite based on a modest accelerating voltage of 20 kV. Supplementary Figure S4 shows the obtained images. The micrographs showed that HAp comprised tiny spherical particles 75–100 nm in diameter.

3.5. Optimization of the adsorption process

- The report of the results analyzed by Design Expert 11

The observed and predicted percentages of Pb^{2+} adsorption by HAp are shown in Supplementary Figure S5 and Table 3.

- Final Equation Using Coded Factors

An actual factor equation can be used to anticipate the reaction to provide amounts for each factor. The mathematical model coded for 16 factorial plans is given by Eq. 15:

$$\%R = 4,16417 + 1,39297 \times A + 0,106589 \times B + 403,009 \times C - 0,0292683 \times A \times B - 3,42483 \times A \times C - 0,295524 \times B \times C - 0,175719 \times A2 + 0,000455118^{*}B2 - 552,174 \times C2. \quad (15)$$

- When comparing the factor coefficients, the coded equation fit well; thus, it can be used to determine the relative importance of the factors. Table 4 shows the results of the analysis of variance (ANOVA) of the interaction factors affecting Pb^{2+} removal.

Fixed-Effects

The degree of freedom for each source is listed in the "df" column. The total degrees of freedom, according to surface methodology, were equal to the number of model coefficients added sequentially line by line.

Model terms were significant when the *p*-value was <0.0500 (Hsissou et al., 2020c). The significant model terms in this situation were a, C, ab, bC, b^2, and C^2. Values >0.1000 imply that the model terms are not significant. If numerous inconsequential model terms (except those required to support hierarchy) are present, model reduction may improve the studied model.

- Optimization

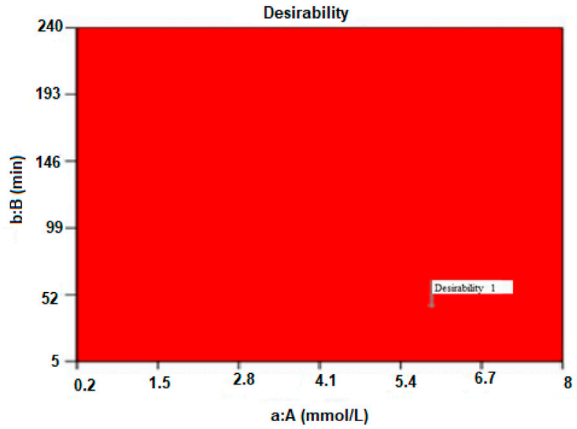

FIGURE 2
Desirability of Pb^{2+} adsorption by HAp.

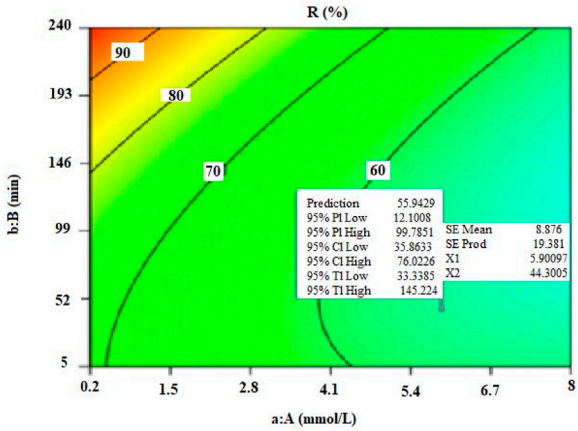

FIGURE 3
Optimized responses of Pb^{2+} removal.

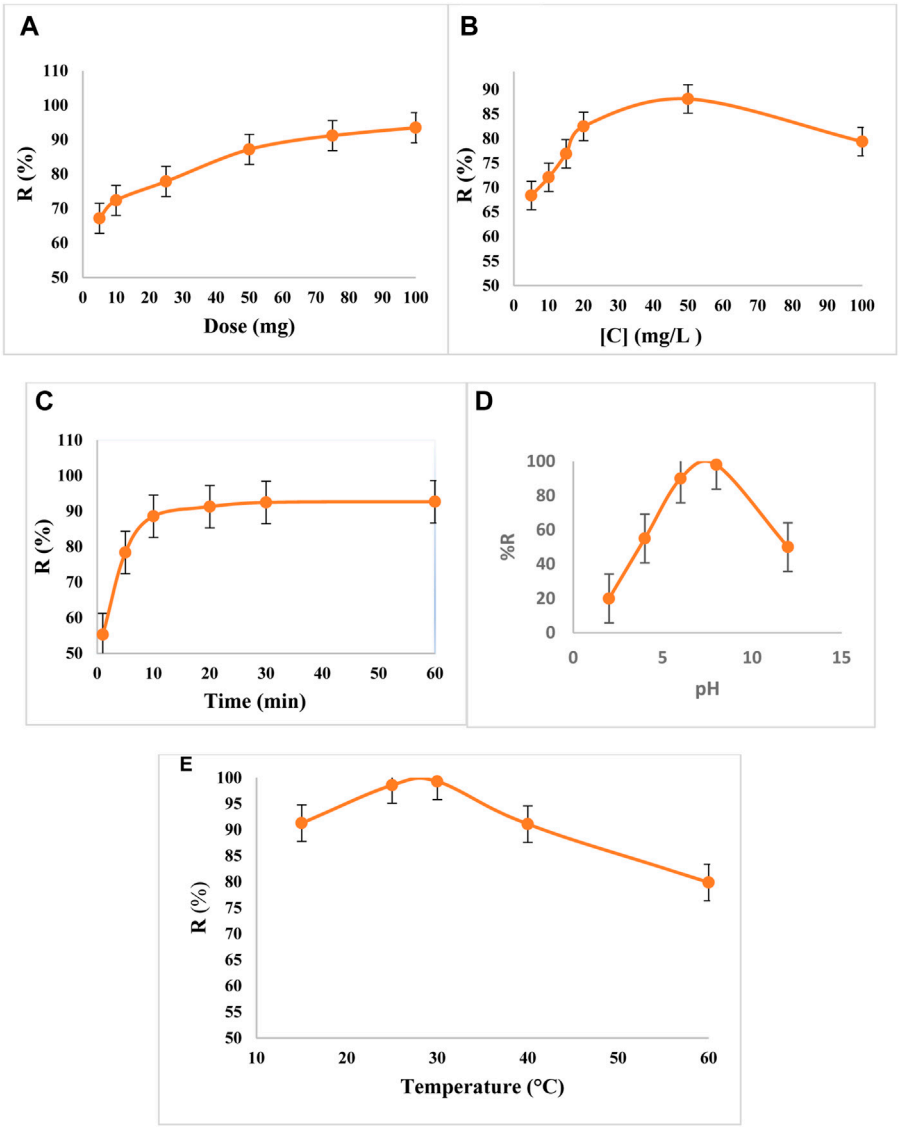

FIGURE 4
Effects of absorption on metal removal by **(A)** adsorbent dose, **(B)** initial Pb^{2+} concentration, **(C)** time, **(D)** pH, and **(E)** temperature.

A desirability function method was performed to optimize the various parameters during the adsorption process (Dagdag et al., 2019), including the initial Pb^{2+} concentration, HAp mass, and contact time. Figure 2 and Figure 3 show the desirability of HAp and the optimized response, respectively.

To achieve maximum desirability, the optimum contact time was 44.3695 min, whereas the adsorbent dose and initial Pb^{2+} concentration were 5.90037 mmol/L, and 0.23233 g, respectively. Fixing these factors showed 98.94% Pb^{2+} elimination.

3.6 Adsorption mechanism

Previous studies on the adsorption of metals in aqueous ion solutions for HAp-based compounds reported ion exchange with Pb^{2+} of the solid (Hsissou et al., 2019). When large concentrations of ions are present, the elimination process usually proceeds using a mechanism other than diffusion, which is described by dissolution-precipitation. HAp may be used to remove lead from contaminated aqueous solutions (Abbout et al., 2020). Other studies reported that Pb^{2+} sorption and removal by HAp is limited to a superficial phenomenon (Dagdag et al., 2020). The adsorption and removal of ions like lead by HAp could employ a combination of three or more mechanisms (Tang et al., 2022).

- In the case of ion exchange between metal ions in the polluted solution and the Pb^{2+} ions in the solid phase, ion exchange occurs by apatite dissolution immediately followed by precipitation, as shown in Eq. 16:

$$Ca_{10}(PO_4)_6(OH)_2 + xM^{2+} \rightarrow Ca_{10-}M_xPO_4)_6(OH)_2 + xCa^{2+} \quad (16)$$

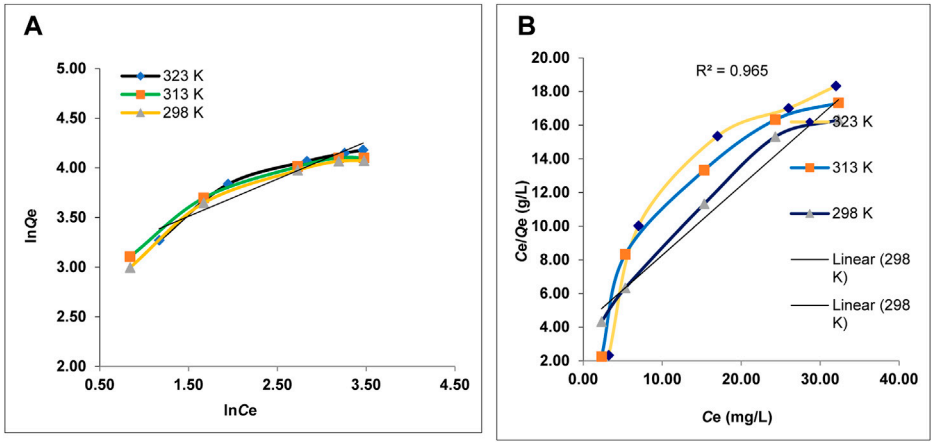

FIGURE 5
Freundlich **(A)** and Langmuir **(B)** adsorption models of Pb^{2+} on HAp at different temperatures.

TABLE 5 Langmuir and Freundlich parameters for the adsorption of Pb^{2+} by HAp.

T (K)		Pb^{2+}		
		298	313	323
Langmuir isotherm	Q (mg/g)	85.92	87.08	90.18
	K_L (L/mg)	1.10	0.99	1.12
	R^2	0.93	0.92	0.96
Freundlich isotherm	$1/n$	0.77	0.74	0.82
	K_F (L/mg)	23.88	26.22	24.36
	R^2	0.81	0.87	0.85

The process can occur not only when these metal ions are exchanged with Pb^{2+} on apatite but also may be adsorbed or attached to the surface during preexisting cationic gaps.

- The other mechanism is metal ion complexation on the surface of Hap followed by dissolution-precipitation.

In this situation, the metal ion removal consists of two steps: HAp dissolution followed by precipitation of a metal phosphate according to Eqs 17, 18:

$$Ca_{10}(PO_4)_6(OH)_2 + 12H^+ \rightarrow 10Ca^{2+} + 6H_2PO^{4-} + 2OH^- \text{ (dissolution)} \quad (17)$$

$$10M^{2+} + 6H_2PO^{4-} + 2OH^- \rightarrow M_{10}(PO4)_6(OH)_2 + 12H^+ \text{ (precipitation)} \quad (18)$$

The hyperbolic shape of the Langmuir isotherm plot increases asymptotically to a constant value. According to the Langmuir classification, this curve represents a type I isotherm. Thus, the matrices may adsorb a single layer of adsorbate. After the first layer, the solute-solvent interactions exceed the solute-surface interaction.

3.7 Metal ion removal

The synthesized HAp was used in a batch adsorption process to study Pb^{+2} removal. The evaluation of the filtrate enables the identification of uncontrolled ions. In a thermostatic bath, HAp adsorbent was suspended in the aqueous metal ion solution with shaking. The influences of adsorbent dose, removal time, temperature, and pH were studied to determine the optimal adsorption conditions. The removal procedure was performed using 50 ml beakers with shaking in a water bath. A portion of the resulting mixture was mixture was filtered through a 0.45 µm syringe filter and assessed by flame atomic absorption at 213.9 and 324.8 nm, respectively.

3.7.1 Effect of adsorbent dosage

A Pb^{+2} concentration of 30 mg/L in 50 ml and a pH of 8 was used to determine the effect of adsorbent dosage with an adsorption duration of 60 min. Figure 4A shows the effect of adsorbent dose on the sorption process, with an optimal absorption observed for 2.0 mg/ml of absorbent. This can be explained by two mechanisms; namely, diffusion and surface coordination. When the adsorbent dose increases, so does the number of binding sites on the surface and the removal effectiveness. Diffusion occurs when the surface sites are all covered and is mostly regulated by the osmosis effect.

3.7.2 Effect of Pb^{+2} Initial Concentration

The adsorbent has a maximum adsorption capacity for Pb^{+2} due to its limited adsorption sites on its surface; there is a suitable initial concentration to start with, to achieve the optimum removal as a high percentage of removal by plotting it as a function of the initial concentration of Pb^{+2}. This was accomplished by using A 0.2 g of the Hap was weighed and immersed in a 50 mL Pb^{2+} solution of varying concentrations at a pH level of 8 and shaken at 150 rpm for 15 min. The maximum removal was 90.37% at the initial concentration of 50 mg L^{-1} (Figure 4B).

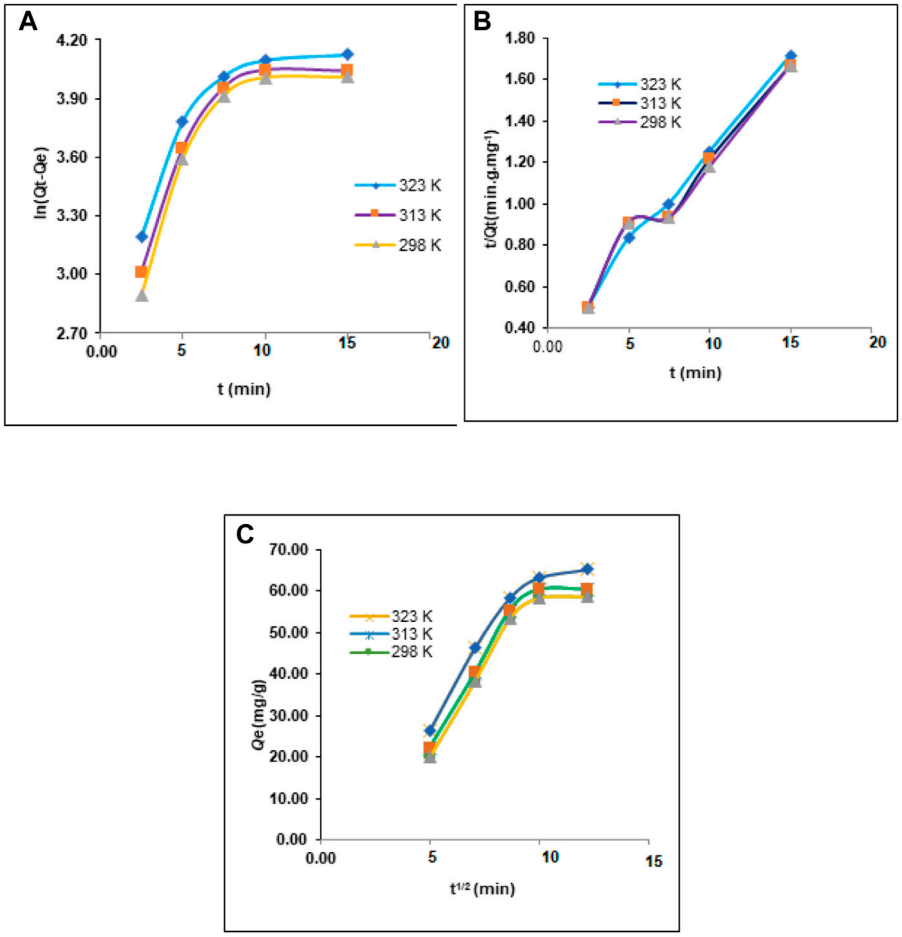

FIGURE 6
(A) Pseudo first-order model of Pb^{2+}adsorption. **(B)** Pseudo second-order model of Pb^{2+}adsorption. **(C)** Intraparticle diffusion model for Pb^{2+} adsorption onto HAp at different temperatures.

3.7.3 Effect of time

The adsorption of Pb^{2+} by the HAp polymer composite base against time was studied at room temperature with an initial concentration of 30 mg/L and an adsorbent dose of 2.0 mg/ml Figure 4C shows that the adsorption rate of the deposited metal ions increased quickly during the first 10 min due to the presence of coordination sites, followed by a decrease for the next 11 min. Equilibrium was then attained, indicating that all the coordination sites were occupied. A contact time of 15 min was optimal.

3.7.4 Effect of pH

To determine the effect of pH on the removal of Pb^{2+} by HAp substrates, an experimental procedure was performed at 25°C. The adsorption was tested in a pH range of 3.0–12. The maximum effectiveness in Pb^{2+} removal from water was observed at a pH of 8 (Figure 4D). For HAp, the proportion of Pb^{2+} elimination at pH 8 was quantifiable, possibly because the active sites on HAp are negatively charged at high pH values, implying that a greater electron density creates a larger dipole interaction between the adsorbent and the Pb^{2+} cation. Other kinds of adsorption, such as ion exchange, may also be involved.

3.7.5 Effect of temperature

The effect of solution temperature on removal efficiency by HAp was investigated in the range of 15°C–60°C. Temperatures of 15°C and 25°C showed slight changes in removal efficiency when the temperature was lowered from 25°C to 15°C during the increase in concentration from 10 to 30 mg/L (Figure 4E). This may have occurred due to the increased rate of diffusion of Pb^{2+} during the increase in temperature to 30°C. The adsorption process was almost exothermic, which makes the adsorption more favorable at low temperatures.

3.8 Adsorption analysis

The adsorption equilibrium between the Pb^{2+} ion solution and HAp was investigated using the Langmuir (Eq. 3) and Freundlich

TABLE 6 Pseudo-first-order model for the adsorption of Pb^{2+} onto HAp.

T (K)	298			313			323		
	K_1 (min^{-1})	Q_e (mg/g)	R^2	K_1 (min^{-1})	Q_e (mg/g)	R^2	K_1 (min^{-1})	Q_e (mg/g)	R^2
Pb^{2+}	0.42	15.38	0.66	0.44	17.30	0.68	0.48	17.20	0.68
Pseudo-second-order model for the adsorption of Pb^{2+} onto HAp.									
T (K)	298			313			323		
	K_2 (g/mg.min)	Q_{cal} (mg/g)	R^2	K_2 (g/mg.min)	Q_{cal} (mg/g)	R^2	K_2 (g/mg.min)	Q_{cal} (mg/g)	R^2
Pb^{2+}	0.05	2.67	0.93	0.14	15.25	0.96	0.18	20.80	0.97
Parameters explaining the intra-particle diffusion of Pb^{2+} onto HAp.									
T (K)	298			313			323		
	K_{id}	Z	R^2	K_{id}	Z	R^2	K_{id}	Z	R^2
Pb^{2+}	27.26	0.81	0.85	27.14	5.27	0.87	27.14	5.27	0.87
Thermodynamic parameters for the adsorption of Pb^{2+} onto HAp.									
T(K)	Pb^{2+}								
	ΔG° (KJ/mol)			ΔH° (KJ/mol)			ΔS° (J/K.mol)		
298	-18.61			17.49			62.53		
313	-19.55								
323	-20.18								
Liquid film diffusion model									
	K_{df}			R^2					
Pb^{2+}	2.07			0.99					

isotherm (Eq. 5) models. Both models were used to evaluate metal ion dispersion on the HAp surface once equilibrium was attained at a constant temperature. Various isotherm models may be used at all temperatures, such as Langmuir, Freundlich, and others. All these models may be used with equations, and the data will fit into these equations. The coefficient of determination (R^2) is one parameter that might influence the kind of isotherm model (Hanbali et al., 2020a).

The adjustment parameters are summarized in Figure 5. The Freundlich isothermal model coefficients of determination are less than those of the Langmuir isothermal model (Table 5), indicating that Pb^{2+} adsorption followed the Langmuir isothermal model, in which Pb^{2+} cations are distributed and present equally and homogeneously across the porous surfaces of the HAp. The separation factor R_L, determined for different doses of adsorbent, varied from $0 < R_L < 1$. Table 5 demonstrates the strong affinity of HAp for the metal ions.

The value of activation energy, Ea, obtained from the Arrhenius equation determines the type of sorption (chemisorption or physical). The Ea was 30.8 kJ/mol; as this value is >20 kJ/mol, chemisorption occurs.

3.8.1 Adsorption kinetics of Pb^{2+} on HAp

The pseudo-second-order model describes the mechanism of Pb^{2+} adsorption in an aqueous solution by presenting data using kinetics equations similar to those of the pseudo-first-order model. These investigations provide information on the probable mechanism of Pb^{2+} adsorption and several transition states in the final complex of Pb^{2+} and adsorbents. Adsorption dynamics may be deduced from reaction parameters such as rate constants and adsorption capacity factors, which will aid the industry in future applications.

To determine the nature of the adsorption process, the adsorption tests of Pb^{2+} by the composite based on HAp were examined using the most common kinetic models. Metal adsorption by solid adsorbents such as HAp composites was modeled using one of the most common kinetic models, pseudo-first order, and pseudo-second-order models. Eqs 7, 8 depict these kinetic models (Khalaf et al., 2021). Weber and Morris devised an equation to describe intraparticle diffusion, as represented in Figure 6.

Table 6 and Figure 6 show the values of the parameters of the aforementioned equations. The plots of ln (Q_e-Q_t) *versus* t

TABLE 7 Previous studies on lead removal from water.

Adsorbent	Optimum condition	Percentage removal (%) or adsorption capacity (qm)	References
Nano-hydroxyapatite modified biochar		63.04 mg g−1	(Ahmed et al., 2022)
Carbonate hydroxyapatite	pH 6.0	101 mg g−1	(Liao et al., 2010)
	60 min		
Chitosan/Fe-hydroxyapatite	Pb initial concentration = 999.4 mg g−1	1,385 mg g−1	(Saber-Samandari et al., 2014)
	70°C		
Magnetic hydroxyapatite/Fe_3O_4	pH = 3.0	440 mg g−1	(Zhuang et al., 2015)
	1 h		
Hydroxyapatite gel	80°C atmospheric pressure	750 mg g−1	(Minh et al., 2013)
hydroxyapatite nano-material prepared from phosphogypsum waste	Initial Pb concentration 50 mg/L	769.23 mg g−1	(Mousa et al., 2016)
	5 min	97.8%	
	0.5 g/L adsorbent weight		
Graphene oxide (GO)	24 h pH = 5.5	2.27 mmol g-1	(Wang et al., 2015)
	2.27 mmol g-1adsorbent weight		
EDTA-GO	20 h pH = 6.8	479 ± 46 mmol/g	(Madadrang et al., 2012)
	0.2 mg g-1 adsorbent weight		
Lignosulfonate-GP –polyaniline (LS-GO-PANI)	60 min pH = 5	216.4 mg g-1	(Yang et al., 2011)
	1.6 g L -1 adsorbent weight		
Graphene/1-octyl-3-methyl-imidazolium hexafluorophosphate	240 min pH = 5.5	74.18–405.9 mg g-1	(Du et al., 2017)
	15 mg L -1 adsorbent weight		
Lignin-grafted carbon nanotubes	120 min pH = 5.8	199 mg g-1	Da'na (2017)
	10 mg L -1 adsorbent weight		
Acid activated bentonite clay	1g/50 ml adsorbent weight	92.85 mg g-1	(Budsaereechai et al., 2012)
	100–5,000 mg L-1concentration		
Peepul tree leaves	25°C pH = 4	127.34 mg g-1	(Gupta et al., 2009)
	1 g L -1 adsorbent weight		
Natural clays	25°C pH = 4.5	90%	(Ahrouch et al., 2019)
Honeycomb monoliths	10–200 mg L -1 adsorbent concentration		
	0.6–200.0 gL-1 adsorbent dose		
Dijah-Monkin	25°C pH = 5.1	8.7 mg g-1	(Alexander et al., 2018)
Bentonite clay	10–50 mg L -1 adsorbent concentration		
	1 gL-1 adsorbent dose		
Ferric activated	25°C pH = 4–6	98.5%	(Yang X et al., 2019)
Biological sludge	50 mg L -1 adsorbent concentration		
	0.5–3 gL-1 adsorbent dose		

(Continued on following page)

TABLE 7 (*Continued*) Previous studies on lead removal from water.

Adsorbent	Optimum condition	Percentage removal (%) or adsorption capacity (qm)	References
Nano-ZnO/yeast composites	25°C pH = 6	66.7 mgg-1	(Zhang et al., 2020)
	25–250 mg L -1 adsorbent concentration		
	4 gL-1 adsorbent dose		
Xanthan biopolymer	30°C–70°C pH = 5.2	80.8%	(Lai et al., 2020)
Integrated	10–300 mg L -1 adsorbent concentration		
graphene	0.1–1 gL-1 adsorbent dose		
Oxide			
Iron oxide modified	25°C pH = 4.5	95%	(Pawar et al., 2018)
Clay activated			
Carbon	12–350 mg L -1 adsorbent concentration		
Composite beads	2 gL-1 adsorbent dose		
Our study (Hap)	25°C pH = 8	98.94%	
	15 min		
	50 mg L -1 adsorbate concentration		

(Figure 6A) provide the value for K_1, whilst the slope and intercept of the plot of t/Qt *versus* t (Figure 6B) supply the values for K_2. The adsorption capacity Q_e, K_{id}, and Z were deduced by tracing Q_t vs. $t^{1/2}$ (Figure 6C).

The experimental results revealed that the pseudo-second-order kinetics model had a higher R^2 (0.93–0.97) than that of the pseudo-first-order kinetics model (0.680). The estimated Q_e values (2.675, 15.252, and 20.856 mg/g) were comparable to the observed Q_e values (2.133, 13.91, and 18.786 mg/g) for the pseudo-second-order model, showing that Pb^{2+} adsorption on the surfaces of HAp conformed to the pseudo-second-order model (Table 7 and Figure 6B).

From Figure 6C (Qt vs. $t^{1/2}$), K_{id} and Z were computed (Table 6). All the graphs in Figure 6 are straight lines that do not cross the origin, showing the presence of several rate-limiting processes.

Accordingly, based on the linearity of the initial graphs shown in Figure 6B we deduced that the adsorption of Pb^{2+} on HAp begins with an immediate adsorption phase (on the outer external surface), which produces chemical adsorption between the metal ions and OH^- and additional functionality (Algarra et al., 2022). The other steps were equally linear, demonstrating the gradual adsorption of Pb^{2+} ions and the step of restricting the rate of intraparticle diffusion.

Table 6 shows that the Z values expanded in the top layer and decreased in the outer mass transfer potential, whereas the inner mass transfer potential increased. The activation energy of the adsorption process was calculated at 298 K and 323 K using Eq. 9.

These findings are significant in improving the understanding of how temperature affects the adsorption of Pb^{2+} on HAp. The calculated activation energy was almost negligible, indicating spontaneous adsorption.

3.8.2 Thermodynamics study

Different thermodynamic parameters have been studied to better understand the type of adsorption based on Eqs 12–14 (Akartasse et al., 2017).

The (ΔG_0) (J mol^{-1}) value was determined according to Eq. 12. Then, ln K_s vs. 1/T was mapped as shown in Supplementary Figure S6, and the slopes and crossings were used to calculate the thermodynamics parameters, as shown in Table 6.

The ΔS^0 and ΔH^0 values are positive, while the entropy at the solid/solution interface is caused by the adsorption process. Furthermore, all free energies for the HAp were negative, indicating spontaneous adsorption at different temperatures.

Metal adsorption generally occurs in different stages. Initially, metal ions start moving from most of the solution to the HAp outer surface. The ions then diffuse across the boundary layer to the HAp outer surface, followed by their adsorption at active sites on the HAp surface and, finally, intraparticle diffusion and ion adsorption across HAp particles. Thus, the liquid film and intraparticle diffusion models were used to explore the sorption mechanism.

According to the liquid film diffusion model, the longest phase of the adsorption process is the flow of adsorbate particles through a liquid film surrounding the solid adsorbent (i.e., the one used to determine the kinetics and interaction of the velocity processes). The liquid film diffusion model is described by Eq. 11:

As mentioned before, F is the fractional attainment of equilibrium, ($F = Q_t/Q_e$), and k_{fd} (min^{-1}) is the film-diffusion coefficient. A linear plot of ln (1 - F) *versus* t with a zero intercept indicates that the kinetics of the adsorption process is governed by diffusion through the liquid film encapsulating HAp. Q_e is the adsorption capacity at equilibrium (mg. g^{-1}).

Supplementary Figure S7 shows that the analytical results of Pb^{2+} adsorption by HAp from aqueous solution at different temperatures did not converge, did not exhibit linear lines crossing the origin, and had very low R^2 values of 0.1876 and 0.1578 for Pb^{2+}, respectively. The diffusion model of the liquid film implies that the diffusion of ions that occurred around the HAp liquid film did not dictate the velocity. However, the liquid film diffusion model occurred at the first few sites during 10 min of sorption, which indicated marginal R^2 of Pb^{+2} increases to 0.9735 and 0.9873, respectively. This finding implied that the diffusion pattern of the liquid film was not the slowest step for rate determination, even if it has a major initial effect on the adsorption (Table 6).

Table 7 shows previous studies on lead. Our results showed 98.94% removal.

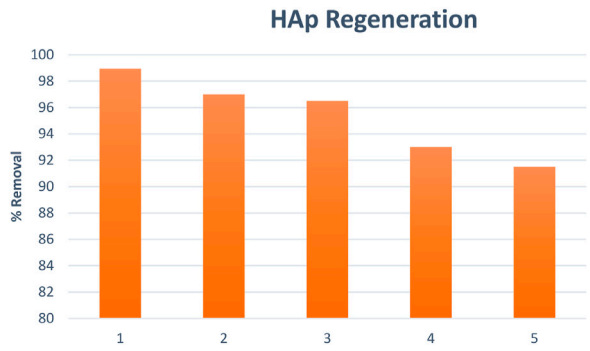

FIGURE 7
Regeneration of HAp for the removal of Pb^{+2}.

3.9 DFT results

Supplementary Figure S8 depicts the HAp geometry before (a.) and after (b.) Pb^{2+} ion adsorption. Due to the strong interactions, the Pb(II) ions are close to the HAp surface, r $[(Pb_{(II)}\text{-}O_{(surface)}]$ = 2.52 Å. The calculated adsorption energy from DFT is -77.25 kcal/mol.

Monte Carlo and molecular dynamics

For the different energy outputs to be calculated, the best arrangement of adsorbate molecules on the surface of the adsorbent must be found. With this method, the adsorption energies can be calculated based on how the adsorbate molecules react with the adsorbent surface. Quantitatively, this is done using the equation below to calculate the adsorption energy (Eads) (Hasani et al., 2022; Sadiku et al., 2022):

$$E_{adsorption} = E_{Adsorbent\ Surface/\mathbf{Pb(II)}} - \left(E_{Adsorbent\ Surface} + E_{Pb(II)}\right) \quad (19)$$

where $E_{Adsorbent\ surface/\mathbf{Tenofovir}}$ is the total energy of the simulated adsorption system and Pb(II) and $Adsorbent\ Surface$ are the total energy of the adsorbate ion and adsorbent, respectively.

MC calculations are used to assess how Pb^{2+} ions adhere to the HAp surface. This way of evaluating the molecule complexity is based on the fact that many combinations of different species (molecules, ions) used in the simulation box are made by chance (Liao et al., 2010). Supplementary Figure S9 shows how the energies of the most favorable or low-energy adsorption sites of adsorbates near the surface of the adsorbent change over time, as determined by running many random Monte Carlo simulations. Supplementary Figure S10 shows how the adsorbate molecules stick to the surface.

The results of the experiment were corroborated by the observation of a significantly higher negative E_{ads} value for the adsorbate molecules as they bound to the surface of the adsorbent (Ben Hadj Ayed et al., 2019). The technique for determining the dynamics of the adsorbate on the material's surface is used in MD simulations (Saber-Samandari et al., 2014). Supplementary Figure S10 shows the final structure of the adsorbate molecules on the Pb(II) surface during MD. Monitoring temperature shifts during the MD simulation may be used to ensure that molecules contain the minimum energy that is practically possible. Supplementary Figure S11 demonstrates that any temperature differences were evidence of the effectiveness of the MD of our system (Ajebli et al., 2022; Babas et al., 2022).

As revealed by their comparably hefty adsorption negative energy and their nearness to the surface (Supplementary Figure S12 on the RDF graph), Pb(II) ions interacted strongly with the adsorbent surface (adsorption geometries in Supplementary Figure S9) (Ajebli et al., 2022).

3.10 Adsorbent regeneration

Figure 7 shows the effect of adsorbent recovery of Pb^{+2} adsorption by HAp. HAp was recycled for five continuous adsorption and desorption cycles, in which the efficiency decreased from 98.94% to 91.5%, indicating that several rounds of adsorbent regeneration can be performed.

Conclusion

The results of this study demonstrated the efficacy of HAp as an adsorbent for the removal of the Pb^{2+}heavy metal from aqueous solutions. The characterization of HAp functional groups as amine and hydroxyl groups revealed that HAp is an excellent absorbent for Pb^{2+} removal. In applying the experimental plan in Design Expert 11 software, studied the effects of independent parameters including initial Pb^{2+} concentration, contact time, and HAp mass on adsorption and interpreted the findings *via* the quadratic polynomial model. The maximum Pb^{+2} removal (98.94%) was obtained for an initial concentration of 50 mg/L and a contact time of 30 min. The adsorption isotherm of Pb^{+2} was consistent with the Langmuir model. The isotherm findings indicated the preferential monolayer adsorption and Pb^{2+} ion adsorption at pH = 8, with adsorption most likely occurring on uncharged sites on the composite surfaces, such as amine and hydroxyl groups. Various kinetic models were also implemented to predict the suitable adsorption mechanism, in which the experimental data fitted well to the pseudo second-order kinetic model. The results

of the thermodynamics study showed that the process was exothermic and spontaneous. Furthermore, the experimental data was confirmed by sophisticated theoretical calculations based on molecular (MC and MD) and quantum mechanics (DFT). The negative adsorption energies and RDF values suggested that Pb(II) ions interacted substantially with the surface of this adsorbent.

Data availability statement

The raw data supporting the conclusion of this article will be made available by the authors, without undue reservation.

Author contributions

LE, SL, KA, and OB did most of the experimental work. SS, AK, AB, and AS helped in FTIR and SEM analysis. SJ, BH, MK, RS, and GH helped in writing and editing the manuscript. AB did the theoretical study.

All authors contributed to the article and approved the submitted version.

Acknowledgments

The authors would like to thank MMK, Chemical Sciences, Faculty of Science, Universiti Brunei Darussalam, Brunei Darussalam, and Department of *Chemistry*, Faculty of Sciences, Mohammed V University in Rabat Morocco, the department of *Chemistry* at Mohammed Premier University and An-Najah National University in Nablus for their help in writing and sample characterization respectively. AB thanks and acknowledges the help from the Ministry of Education, Science and Technology of Kosovo (Nr.2-5069) for providing the computing resources. Special thanks goes to Merc Project No: M35-018. The Project title: Residuals of Pharmaceuticals and Personal Care Products in Wastewater, Uptake in Vegetables and Fruits versus Pesticide Residuals: Evaluating Health Risks and Treatment Strategies. This work was in part supported by the research project "Palestinian German Scientific Bridge (PGSB)" carried out by the Forschungszentrum Jülich and Palestinian Academy for Science and Technology-PALAST and funded by the German Federal Ministry of Education and Research (BMBF).

Conflict of interest

The authors declare that the research was conducted in the absence of any commercial or financial relationships that could be construed as a potential conflict of interest.

Publisher's note

All claims expressed in this article are solely those of the authors and do not necessarily represent those of their affiliated organizations, or those of the publisher, the editors, and the reviewers. Any product that may be evaluated in this article, or claim that may be made by its manufacturer, is not guaranteed or endorsed by the publisher.

Supplementary material

The Supplementary Material for this article can be found online at: https://www.frontiersin.org/articles/10.3389/fenvs.2023.1112019/full#supplementary-material

References

Abbout, S., Zouarhi, M., Chebabe, D., Damej, M., Berisha, A., and Hajjaji, N. (2020). Galactomannan as a new bio-sourced corrosion inhibitor for iron in acidic media. *Heliyon* 6 (3), e03574. doi:10.1016/j.heliyon.2020.e03574

Abdelwedoud, B. O., Damej, M., Tassaoui, K., Berisha, A., Tachallait, H., Bougrin, K., et al. (2022). Inhibition effect of N-propargyl saccharin as corrosion inhibitor of C38 steel in 1 M HCl, experimental and theoretical study. *J. Mol. Liq.* 354, 118784. doi:10.1016/j.molliq.2022.118784

Ahmed, W., Xu, T., Mahmood, M., Núñez-Delgado, A., Ali, S., Shakoor, A., et al. (2022). Nano-hydroxyapatite modified biochar: Insights into the dynamic adsorption and performance of lead (II) removal from aqueous solution. *Environ. Res.* 214, 113827. doi:10.1016/j.envres.2022.113827

Ahrouch, M., Gatica, J. M., Draoui, K., Bellido, D., and Vidal, H. (2019). Lead removal from aqueous solution by means of integral natural clays honeycomb monoliths. *J. Hazard. Mater.* 365, 519–530. doi:10.1016/j.jhazmat.2018.11.037

Ajebli, S., Kaichouh, G., Khachani, M., Babas, H., El Karbane, M., Warad, I., et al. (2022). The adsorption of Tenofovir in aqueous solution on activated carbon produced from maize cobs: Insights from experimental, molecular dynamics simulation, and DFT calculations. *Chem. Phys. Lett.* 801, 139676. doi:10.1016/j.cplett.2022.139676

Ajibade, F. O., Adelodun, B., Lasisi, K. H., Fadare, O. O., Ajibade, T. F., Nwogwu, N. A., et al. (2021). "Environmental pollution and their socioeconomic impacts," in *Microbe mediated remediation of environmental contaminants* (Elsevier), 321–354.

Akartasse, N., Mejdoubi, E., Razzouki, B., Azzaoui, K., Jodeh, S., Hamed, O., et al. (2017). Natural product based composite for extraction of arsenic (III) from waste water. *Chem. Central J.* 11 (1), 33–13. doi:10.1186/s13065-017-0261-9

Alexander, J. A., Ahmad Zaini, M. A., Surajudeen, A., Aliyu, E.-N. U., and Omeiza, A. U. (2018). Insight into kinetics and thermodynamics properties of multicomponent lead (II), cadmium (II) and manganese (II) adsorption onto Dijah-Monkin bentonite clay. *Part. Sci. Technol.* 36 (5), 569–577. doi:10.1080/02726351.2016.1276499

Algarra, M., Jodeh, S., Aqel, I., Hanbali, G., Radi, S., Tighadouini, S., et al. (2022). Phenylamine/amide grafted in silica as sensing Nanocomposites for the removal of carbamazepine: A DFT approach. *Chemosensors* 10 (2), 76. doi:10.3390/chemosensors10020076

Azzaoui, K., Lamhamdi, A., Mejdoubi, E., Berrabah, M., Elidrissi, A., Hammouti, B., et al. (2013). Synthesis of nanostructured hydroxyapatite in presence of polyethylene glycol 1000. *J. Chem. Pharm. Res.* 5 (12), 1209–1216.

Babas, H., Khachani, M., Warad, I., Ajebli, S., Guessous, A., Guenbour, A., et al. (2022). Sofosbuvir adsorption onto activated carbon derived from argan shell residue: Optimization, kinetic, thermodynamic and theoretical approaches. *J. Mol. Liq.* 356, 119019. doi:10.1016/j.molliq.2022.119019

Barone, V., and Cossi, M. (1998). Quantum calculation of molecular energies and energy gradients in solution by a conductor solvent model. *J. Phys. Chem. A* 102 (11), 1995–2001. doi:10.1021/jp9716997

Ben Hadj Ayed, M., Osmani, T., Issaoui, N., Berisha, A., Oujia, B., and Ghalla, H. (2019). Structures and relative stabilities of Na+ Nen (n= 1–16) clusters via pairwise and DFT calculations. *Theor. Chem. Accounts* 138 (7), 84–12. doi:10.1007/s00214-019-2476-4

Berisha, A., Combellas, C., Kanoufi, F., Decorse, P., Oturan, N., Médard, J., et al. (2017). Some theoretical and experimental insights on the mechanistic routes leading to the spontaneous grafting of gold surfaces by diazonium salts. *Langmuir* 33 (35), 8730–8738. doi:10.1021/acs.langmuir.7b01371

Berisha, A. (2019). Interactions between the aryldiazonium cations and graphene oxide: A DFT study. *J. Chem.* 2019, 1–5. doi:10.1155/2019/5126071

Berisha, A. (2021). First principles details into the grafting of aryl radicals onto the free-standing and borophene/Ag (1 1 1) surfaces. *Chem. Phys.* 544, 111124. doi:10.1016/j.chemphys.2021.111124

Berisha, A., and Seydou, M. (2022). "Grafting of aryl radicals onto surfaces—a DFT study," in *Aryl diazonium salts and related compounds* (Springer), 121–135.

Budsaereechai, S., Kamwialisak, K., and Ngernyen, Y. (2012). Adsorption of lead, cadmium and copper on natural and acid activated bentonite clay. *Asia-Pacific J. Sci. Technol.* 17 (5), 800–810.

Chen, Q., Yao, Y., Li, X., Lu, J., Zhou, J., and Huang, Z. (2018). Comparison of heavy metal removals from aqueous solutions by chemical precipitation and characteristics of precipitates. *J. water process Eng.* 26, 289–300. doi:10.1016/j.jwpe.2018.11.003

Da'na, E. (2017). Adsorption of heavy metals on functionalized-mesoporous silica: A review. *Microporous Mesoporous Mater.* 247, 145–157. doi:10.1016/j.micromeso.2017.03.050

Dagdag, O., Hsissou, R., Berisha, A., Erramli, H., Hamed, O., Jodeh, S., et al. (2019). Polymeric-based epoxy cured with a polyaminoamide as an anticorrosive coating for aluminum 2024-T3 surface: Experimental studies supported by computational modeling. *J. Bio-and Tribo-Corrosion* 5 (3), 58–13. doi:10.1007/s40735-019-0251-7

Dagdag, O., Hsissou, R., El Harfi, A., Berisha, A., Safi, Z., Verma, C., et al. (2020). Fabrication of polymer based epoxy resin as effective anti-corrosive coating for steel: Computational modeling reinforced experimental studies. *Surfaces Interfaces* 18, 100454. doi:10.1016/j.surfin.2020.100454

Dai, L., Zhao, W., Wei, B., Zhang, K., and Han, T. (2021). Adsorption of Pb2+ by insolubilized humic acid extracted from sewage sludge. *J. Material Cycles Waste Manag.* 23 (3), 1037–1047. doi:10.1007/s10163-021-01193-9

Du, Y., Wang, J., Zou, Y., Yao, W., Hou, J., Xia, L., et al. (2017). Synthesis of molybdenum disulfide/reduced graphene oxide composites for effective removal of Pb (II) from aqueous solutions. *Sci. Bull.* 62 (13), 913–922. doi:10.1016/j.scib.2017.05.025

El Amri, A., Kadiri, L., Hsissou, R., Lebkiri, A., Wardighi, Z., Lebkiri, A., et al. (2023). Investigation of Typha Latifolia (TL) as potential biosorbent for removal of the methyl orange anionic dye in the aqueous solution. Kinetic and DFT approaches. *J. Mol. Struct.* 1272, 134098. doi:10.1016/j.molstruc.2022.134098

El Hammari, L., Laghzizil, A., Saoiabi, A., Barboux, P., and Meyer, M. (2006a). Chemical modification of porous calcium hydroxyapatite surfaces by grafting phenylphosphonic and phenylphosphite acids. *Colloids Surfaces A Physicochem. Eng. Aspects* 289 (1-3), 84–88. doi:10.1016/j.colsurfa.2006.04.009

El Hammari, L., Laghzizil, A., Saoiabi, A., Barboux, P., Meyer, M., Brandes, S., et al. (2006b). Some factors affecting the removal of lead (II) ions from aqueous solution by porous calcium hydroxyapatite: Relationships between surface and adsorption properties. *Adsorpt. Sci. Technol.* 24 (6), 507–516. doi:10.1260/026361706780154419

El Hammari, L., Merroun, H., Coradin, T., Cassaignon, S., Laghzizil, A., and Saoiabi, A. (2007). Mesoporous hydroxyapatites prepared in ethanol–water media: Structure and surface properties. *Mater. Chem. Phys.* 104 (2-3), 448–453. doi:10.1016/j.matchemphys.2007.04.002

El-Bahy, S. M., and El-Bahy, Z. M. (2016). Synthesis and characterization of polyamidoxime chelating resin for adsorption of Cu (II), Mn (II) and Ni (II) by batch and column study. *J. Environ. Chem. Eng.* 4 (1), 276–286. doi:10.1016/j.jece.2015.10.040

Gupta, V. K., Carrott, P. J. M., Ribeiro Carrott, M. M. L., and Suhas (2009). Low-cost adsorbents: Growing approach to wastewater treatment—a review. *Crit. Rev. Environ. Sci. Technol.* 39 (10), 783–842. doi:10.1080/10643380801977610

Hamed, R., Jodeh, S., Hanbali, G., Safi, Z., Berisha, A., Xhaxhiu, K., et al. (2022). Eco-friendly synthesis and characterization of double-crossed Link 3D graphene oxide functionalized with chitosan for adsorption of sulfamethazine from aqueous solution: Experimental and DFT calculations. *Front." Environ. Sci.* 10, 930693. doi:10.3389/fenvs.2022.930693

Hanbali, G., Jodeh, S., Hamed, O., Bol, R., Khalaf, B., Qdemat, A., et al. (2020a). Enhanced ibuprofen adsorption and desorption on synthesized functionalized magnetic multiwall carbon nanotubes from aqueous solution. *Materials* 13 (15), 3329. doi:10.3390/ma13153329

Hanbali, G., Jodeh, S., Hamed, O., Bol, R., Khalaf, B., Qdemat, A., et al. (2020b). Magnetic multiwall carbon nanotube decorated with novel functionalities: Synthesis and application as adsorbents for lead removal from aqueous medium. *Processes* 8 (8), 986. doi:10.3390/pr8080986

Hasani, N., Selimi, T., Mele, A., Thaçi, V., Halili, J., Berisha, A., et al. (2022). Theoretical, equilibrium, kinetics and thermodynamic investigations of methylene blue adsorption onto lignite coal. *Molecules* 27 (6), 1856. doi:10.3390/molecules27061856

Hsissou, R., Dagdag, O., Abbout, S., Benhiba, F., Berradi, M., El Bouchti, M., et al. (2019). Novel derivative epoxy resin TGETET as a corrosion inhibition of E24 carbon steel in 1.0 M HCl solution. Experimental and computational (DFT and MD simulations) methods. *J. Mol. Liq.* 284, 182–192. doi:10.1016/j.molliq.2019.03.180

Hsissou, R., Abbout, S., Seghiri, R., Rehioui, M., Berisha, A., Erramli, H., et al. (2020a). Evaluation of corrosion inhibition performance of phosphorus polymer for carbon steel in [1 M] HCl: Computational studies (DFT, MC and MD simulations). *J. Mater. Res. Technol.* 9 (3), 2691–2703. doi:10.1016/j.jmrt.2020.01.002

Hsissou, R., Benhiba, F., Abbout, S., Dagdag, O., Benkhaya, S., Berisha, A., et al. (2020b). Trifunctional epoxy polymer as corrosion inhibition material for carbon steel in 1.0 M HCl: MD simulations, DFT and complexation computations. *Inorg. Chem. Commun.* 115, 107858. doi:10.1016/j.inoche.2020.107858

Hsissou, R., Benzidia, B., Rehioui, M., Berradi, M., Berisha, A., Assouag, M., et al. (2020c). Anticorrosive property of hexafunctional epoxy polymer HGTMDAE for E24 carbon steel corrosion in 1.0 M HCl: Gravimetric, electrochemical, surface morphology and molecular dynamic simulations. *Polym. Bull.* 77 (7), 3577–3601. doi:10.1007/s00289-019-02934-5

Hsissou, R., Abbout, S., Safi, Z., Benhiba, F., Wazzan, N., Guo, L., et al. (2021). Synthesis and anticorrosive properties of epoxy polymer for CS in [1 M] HCl solution: Electrochemical, AFM, DFT and MD simulations. *Constr. Build. Mater.* 270, 121454. doi:10.1016/j.conbuildmat.2020.121454

Hsissou, R. (2021). Review on epoxy polymers and its composites as a potential anticorrosive coatings for carbon steel in 3.5% NaCl solution: Computational approaches. *J. Mol. Liq.* 336, 116307. doi:10.1016/j.molliq.2021.116307

Hu, Y., Gao, H., Yang, Q., Zhou, W., and Sun, C. (2022). Adsorption of Pb2+ and Cd2+ on reduced graphene oxide hydrogel prepared from natural cryptocrystalline graphite. *Colloids Surfaces A Physicochem. Eng. Aspects* 642, 128630. doi:10.1016/j.colsurfa.2022.128630

Huang, X., and Pan, M. (2016). Retracted: The highly efficient adsorption of Pb(II) on graphene oxides: A process combined by batch experiments and modeling techniques. *J. Mol. Liq.* 100 (215), 410–416. doi:10.1016/j.molliq.2015.12.061

Kadiri, L., Ouass, A., Hsissou, R., Safi, Z., Wazzan, N., Essaadaoui, Y., et al. (2021). Adsorption properties of coriander seeds: Spectroscopic kinetic thermodynamic and computational approaches. *J. Mol. Liq.* 343, 116971. doi:10.1016/j.molliq.2021.116971

Khalaf, B., Hamed, O., Jodeh, S., Bol, R., Hanbali, G., Safi, Z., et al. (2021). Cellulose-based hectocycle nanopolymers: Synthesis, molecular docking and adsorption of difenoconazole from aqueous medium. *Int. J. Mol. Sci.* 22 (11), 6090. doi:10.3390/ijms22116090

Klamt, A. (2018). The COSMO and COSMO-RS solvation models. *Wiley Interdiscip. Rev. Comput. Mol. Sci.* 8 (1), e1338. doi:10.1002/wcms.1338

Kwak, J.-H., Islam, M. S., Wang, S., Messele, S. A., Naeth, M. A., El-Din, M. G., et al. (2019). Biochar properties and lead (II) adsorption capacity depend on feedstock type, pyrolysis temperature, and steam activation. *Chemosphere* 231, 393–404. doi:10.1016/j.chemosphere.2019.05.128

Lai, K. C., Lee, L. Y., Hiew, B. Y. Z., Thangalazhy-Gopakumar, S., and Gan, S. (2020). Facile synthesis of xanthan biopolymer integrated 3D hierarchical graphene oxide/titanium dioxide composite for adsorptive lead removal in wastewater. *Bioresour. Technol.* 309, 123296. doi:10.1016/j.biortech.2020.123296

Liao, D., Zheng, W., Li, X., Yang, Q., Yue, X., Guo, L., et al. (2010). Removal of lead (II) from aqueous solutions using carbonate hydroxyapatite extracted from eggshell waste. *J. Hazard. Mater.* 177 (1-3), 126–130. doi:10.1016/j.jhazmat.2009.12.005

Madadrang, C. J., Kim, H. Y., Gao, G., Wang, N., Zhu, J., Feng, H., et al. (2012). Adsorption behavior of EDTA-graphene oxide for Pb (II) removal. *ACS Appl. Mater. interfaces* 4 (3), 1186–1193. doi:10.1021/am201645g

Mehana, E.-S. E., Khafaga, A. F., Elblehi, S. S., Abd El-Hack, M. E., Naiel, M. A., Bin-Jumah, M., et al. (2020). Biomonitoring of heavy metal pollution using acanthocephalans parasite in ecosystem: An updated overview. *Animals* 10 (5), 811. doi:10.3390/ani10050811

Minh, D. P., Tran, N. D., Nzihou, A., and Sharrock, P. (2013). Hydroxyapatite gel for the improved removal of Pb2+ ions from aqueous solution. *Chem. Eng. J.* 232, 128–138. doi:10.1016/j.cej.2013.07.086

Mohammed, A. A., Selman, H. M., and abukhanafer, G. (2018). Liquid surfactant membrane for lead separation from aqueous solution: Studies on emulsion stability and extraction efficiency. *J. Environ. Chem. Eng.* 6 (6), 6923–6930. doi:10.1016/j.jece.2018.10.021

Molhi, A., Hsissou, R., Damej, M., Berisha, A., Bamaarouf, M., Seydou, M., et al. (2021). Performance of two epoxy compounds against corrosion of C38 steel in 1 M HCl: Electrochemical, thermodynamic and theoretical assessment. *Int. J. Corros. Scale Inhibition* 10 (2), 812–837. doi:10.17675/2305-6894-2021-10-2-21

Mousa, S., Ammar, N., and Ibrahim, H. (2016). Removal of lead ions using hydroxyapatite nano-material prepared from phosphogypsum waste. *J. Saudi Chem. Soc.* 20 (3), 357–365. doi:10.1016/j.jscs.2014.12.006

Nazari, G., Abolghasemi, H., and Esmaieli, M. (2016). Batch adsorption of cephalexin antibiotic from aqueous solution by walnut shell-based activated carbon. *J. Taiwan Inst. Chem. Eng.* 58, 357–365. doi:10.1016/j.jtice.2015.06.006

Nyairo, W. N., Eker, Y. R., Kowenje, C., Akin, I., Bingol, H., Tor, A., et al. (2018). Efficient adsorption of lead (II) and copper (II) from aqueous phase using oxidized multiwalled carbon nanotubes/polypyrrole composite. *Sep. Sci. Technol.* 53 (10), 1498–1510. doi:10.1080/01496395.2018.1424203

Olatunji-Ojo, A. M., Alimba, C. G., Adenipekun, C. O., and Bakare, A. A. (2020). Experimental simulation of somatic and germ cell genotoxicity in male *Mus musculus* fed extracts of lead contaminated Pleurotus ostreatus (white rot fungi). *Environ. Sci. Pollut. Res.* 27 (16), 19754–19763. doi:10.1007/s11356-020-08494-w

Pawar, R. R., Kim, M., Kim, J.-G., Hong, S.-M., Sawant, S. Y., Lee, S. M., et al. (2018). Efficient removal of hazardous lead, cadmium, and arsenic from aqueous environment

by iron oxide modified clay-activated carbon composite beads. *Appl. Clay Sci.* 162, 339–350. doi:10.1016/j.clay.2018.06.014

Rafatullah, M., Sulaiman, O., Hashim, R., and Ahmad, A. (2010). Adsorption of methylene blue on low-cost adsorbents: A review. *J. Hazard. Mater.* 177 (1-3), 70–80. doi:10.1016/j.jhazmat.2009.12.047

Rahimi, A., Farhadian, A., Berisha, A., Shaabani, A., Varfolomeev, M. A., Mehmeti, V., et al. (2022). Novel sucrose derivative as a thermally stable inhibitor for mild steel corrosion in 15% HCl medium: An experimental and computational study. *Chem. Eng. J.* 446, 136938. doi:10.1016/j.cej.2022.136938

Saber-Samandari, S., Saber-Samandari, S., Nezafati, N., and Yahya, K. (2014). Efficient removal of lead (II) ions and methylene blue from aqueous solution using chitosan/Fe-hydroxyapatite nanocomposite beads. *J. Environ. Manag.* 146, 481–490. doi:10.1016/j.jenvman.2014.08.010

Sadiku, M., Selimi, T., Berisha, A., Maloku, A., Mehmeti, V., Thaçi, V., et al. (2022). Removal of methyl violet from aqueous solution by adsorption onto halloysite nanoclay: Experiment and theory. *Toxics* 10 (8), 445. doi:10.3390/toxics10080445

Said, B., M'rabet, S., Hsissou, R., and El Harfi, A. (2020). Synthesis of new low-cost organic ultrafiltration membrane made from Polysulfone/Polyetherimide blends and its application for soluble azoic dyes removal. *J. Mater. Res. Technol.* 9 (3), 4763–4772. doi:10.1016/j.jmrt.2020.02.102

Saoiabi, S., Achelhi, K., Masse, S., Saoiabi, A., Laghzizil, A., and Coradin, T. (2013). Organo-apatites for lead removal from aqueous solutions: A comparison between carboxylic acid and aminophosphonate surface modification. *Colloids Surfaces A Physicochem. Eng. Aspects* 419, 180–185. doi:10.1016/j.colsurfa.2012.12.005

Saravanan, A., Kumar, P. S., Jeevanantham, S., Karishma, S., Tajsabreen, B., Yaashikaa, P., et al. (2021). Effective water/wastewater treatment methodologies for toxic pollutants removal: Processes and applications towards sustainable development. *Chemosphere* 280, 130595. doi:10.1016/j.chemosphere.2021.130595

Singh, D. V., Bhat, R. A., Upadhyay, A. K., Singh, R., and Singh, D. (2021). Microalgae in aquatic environs: A sustainable approach for remediation of heavy metals and emerging contaminants. *Environ. Technol. Innovation* 21, 101340. doi:10.1016/j.eti.2020.101340

Sruamsiri, D., and Ogawa, M. (2022). "Adsorption of Pb2+ on a layered alkali titanate from water," in *IOP conference series: Earth and environmental science* (Rayong, Thailand: IOP Publishing).

Tang, S.-F., Zhou, H., Tan, W.-T., Huang, J.-G., Zeng, P., Gu, J.-F., et al. (2022). Adsorption characteristics and mechanisms of Fe-Mn oxide modified biochar for Pb (II) in wastewater. *Int. J. Environ. Res. Public Health* 19 (14), 8420. doi:10.3390/ijerph19148420

Ukaogo, P. O., Ewuzie, U., and Onwuka, C. V. (2020). "Environmental pollution: Causes, effects, and the remedies," in *Microorganisms for sustainable environment and health* (Elsevier), 419–429.

Vardhan, K. H., Kumar, P. S., and Panda, R. C. (2019). A review on heavy metal pollution, toxicity and remedial measures: Current trends and future perspectives. *J. Mol. Liq.* 290, 111197. doi:10.1016/j.molliq.2019.111197

Wang, H., Gao, B., Wang, S., Fang, J., Xue, Y., and Yang, K. (2015). Removal of Pb (II), Cu (II), and Cd (II) from aqueous solutions by biochar derived from KMnO4 treated hickory wood. *Bioresour. Technol.* 197, 356–362. doi:10.1016/j.biortech.2015.08.132

Wu, J., Wang, T., Wang, J., Zhang, Y., and Pan, W.-P. (2021). A novel modified method for the efficient removal of Pb and Cd from wastewater by biochar: Enhanced the ion exchange and precipitation capacity. *Sci. Total Environ.* 754, 142150. doi:10.1016/j.scitotenv.2020.142150

Yang, S., Hu, J., Chen, C., Shao, D., and Wang, X. (2011). Mutual effects of Pb (II) and humic acid adsorption on multiwalled carbon nanotubes/polyacrylamide composites from aqueous solutions. *Environ. Sci. Technol.* 45 (8), 3621–3627. doi:10.1021/es104047d

Yang, X., Xu, G., and Yu, H. (2019). Removal of lead from aqueous solutions by ferric activated sludge-based adsorbent derived from biological sludge. *Arabian J. Chem.* 12 (8), 4142–4149. doi:10.1016/j.arabjc.2016.04.017

Yang, Z., Zhou, Y., Feng, Z., Rui, X., Zhang, T., and Zhang, Z. (2019). A review on reverse osmosis and nanofiltration membranes for water purification. *Polymers* 11 (8), 1252. doi:10.3390/polym11081252

Zhang, A., Li, X., Xing, J., and Xu, G. (2020). Adsorption of potentially toxic elements in water by modified biochar: A review. *J. Environ. Chem. Eng.* 8 (4), 104196. doi:10.1016/j.jece.2020.104196

Zhao, Y., and Truhlar, D. G. (2008). The M06 suite of density functionals for main group thermochemistry, thermochemical kinetics, noncovalent interactions, excited states, and transition elements: Two new functionals and systematic testing of four M06-class functionals and 12 other functionals. *Theor. Chem. accounts* 120 (1), 215–241. doi:10.1007/s00214-007-0310-x

Zhuang, F., Tan, R., Shen, W., Zhang, X., Xu, W., and Song, W. (2015). Monodisperse magnetic hydroxyapatite/Fe3O4 microspheres for removal of lead (II) from aqueous solution. *J. Alloys Compd.* 637, 531–537. doi:10.1016/j.jallcom.2015.02.216